

Energy levels of nitride quantum dots: Wurtzite versus zinc-blende structureAnjana Bagga,¹ P. K. Chattopadhyay,² and Subhasis Ghosh¹¹*School of Physical Sciences, Jawaharlal Nehru University, New Delhi 110067, India*²*Department of Physics, Maharshi Dayanand University, Rohtak, India*

(Received 10 April 2003; revised manuscript received 1 August 2003; published 28 October 2003)

Nitride based III-V quantum dots (QD's) GaN, InN, and AlN have been investigated theoretically using the hole effective mass Hamiltonian derived by the $\vec{k}\cdot\vec{p}$ method. The nitride based QD's have significantly different properties compared to II-VI based QD's and also other III-V based QD's such as GaAs and InP. III-V based nitrides can have both zinc blende and wurtzite crystal structures whereas GaAs and other III-V and II-VI QD's exist only in the zinc blende structure. The study of nitride QD's therefore offers an unique opportunity of studying the role of the crystal field which is present in the wurtzite structure and is absent in zinc blende structure. The energies and the eigenfunctions for spherical quantum dots have been calculated as functions of the dot radius R for both zinc blende and wurtzite structures for both the zero spin orbit coupling (SOC) and finite SOC. For low lying states, in the zero SOC limit, the energies have a $1/R^2$ dependence at all R for zinc blende structures but the presence of crystal field in wurtzite modifies the $1/R^2$ dependence at intermediate R but not in small and large R . The addition of SOC further modifies the behavior at large R and the energies vary more slowly than $1/R^2$ for both the zinc blende and wurtzite structures. For very high excited states of large QD's, the wurtzite pattern approaches that of the zinc blende.

DOI: 10.1103/PhysRevB.68.155331

PACS number(s): 73.22.-f, 73.21.La, 72.80.Ey

I. INTRODUCTION

Investigation of semiconductor quantum dots (QD's) or nanocrystals (NC's) reveals the evolution of the electronic structure from the extended solid state to the molecular limit, an extremely important issue of basic and applied research in condensed matter physics. The superior properties of QD based laser,¹ size dependent tunable light emitters, and detectors were recognized early. A single electron transistor² and several many body phenomena, such as the Kondo effect,³ and metal insulator transition⁴ have been observed in nanometer-sized QD's. There has been tremendous progress in the fabrication of self-assembled QD's using the epitaxial method^{5,6} and highly monodispersive QD's using chemical methods^{7,8} with very high quantum efficiency of optical transitions. The field of nitride based III-V QD's is not as mature as II-VI based QD's, such as CdSe, CdS, ZnS, and ZnSe. Most of the reports on GaN QD are concerned with nanopowders embedded in matrices. There are a few reports on the fabrication of GaN-QD using metal organic chemical vapor deposition (MOCVD).^{9,10} Nitride based nanostructures have significantly different properties as compared to GaAs based quantum well and QD's. GaAs and most other III-V semiconductors have zinc blende crystal structure, but III-V nitrides are available in both zinc blende and wurtzite crystal structures which leads to strong built in piezoelectric fields in heterostructures. This can induce large redshifts in GaN/AlN self-organized QD's.^{11,12} Recently, nitride based QD's have become a field of active interest. It has been proposed that InGaN is a truly quantum material.¹ The origin of its high quantum efficiency of luminescence, despite the large density of structural defects, lies with the phase separable nearly pure self-formed InN QD's rather than with the alloy composition.^{13,14} These structures could be practical building blocks for solid state quantum computing devices.¹⁵ The existence of strong inbuilt electric field due to a giant piezo-

electric effect can be utilized to generate entangled exciton-exciton states,¹⁶ required for information processing in quantum computers. In recent years many sophisticated theoretical approaches have been applied on QD's.¹⁷⁻³⁹ These are multiband $\vec{k}\cdot\vec{p}$ theory,¹⁹⁻²⁶ empirical pseudopotential theory,^{30,31} and tight binding methods.³²⁻³⁶ Different theoretical approaches are the manifestation of QD's being intermediate between molecular and bulk systems. Of these, the $\vec{k}\cdot\vec{p}$ method using six or eight bands has several advantages: (i) the method is known to give a good description of the hole states and the crystal field splitting of bands at zone center which are important for determining the optical properties accurately, (ii) the $\vec{k}\cdot\vec{p}$ method is much less computationally demanding compared to other methods, (iii) it is ideally suited for device modeling in particular for the optoelectronic devices, and (iv) theoretically the method is more transparent compared to other numerically demanding methods. Therefore, to understand the electronic properties of nitride based QD's and future QD based devices, the $\vec{k}\cdot\vec{p}$ method is ideally suited. The electronic structure of II-VI (CdS, CdSe, ZnS, and ZnSe) and III-V (InAs, InP, and GaAs) QD's have been widely studied,²¹⁻²⁶ but the electronic structure of nitride (InN, GaN, and AlN) based QD's have not yet been studied theoretically in detail except for the work by Andreev and Reilly¹² who applied the $\vec{k}\cdot\vec{p}$ theory to the GaN/AlN heterostructures with truncated hexagonal pyramids. In this paper we present a realistic multiband calculation of the electronic structures in isolated and unstrained InN, GaN, and AlN QD's for both the wurtzite and zinc blende structure. The $\vec{k}\cdot\vec{p}$ method successfully describes the confined electron and hole states in QD's for both zinc blende and the wurtzite structures. The crystal field splitting is negative for AlN and positive for InN and GaN. Due to the crystal field, in the case of zero SOC, the threefold degeneracy of hole states at the valence band top of zinc

blende structures is broken for wurtzite semiconductors. Since the optical transitions take place from the band edges it is important as well as interesting to systematically work out the evolution of the hole states for QD's due to crystal field splitting. In Sec. II the theoretical framework used in the calculation is given. The results obtained and their discussion will be found in Sec. III. Section IV gives the conclusions.

II. ELECTRONIC STATES IN SPHERICAL QUANTUM DOTS

A. Wurtzite structure

The Hamiltonian in effective-mass theory, for hole states for wurtzite structures in the zero SOC limit is given by²³

$$H_0 = \frac{1}{2m_0} \begin{pmatrix} Lp_x^2 + Mp_y^2 + Np_z^2 & Rp_xp_y & Qp_xp_z + \Lambda p_0p_x \\ Rp_xp_y & Lp_y^2 + Mp_x^2 + Np_z^2 & Qp_y p_z + \Lambda p_0p_y \\ Qp_y p_z + \Lambda p_0p_y & Qp_y p_z + \Lambda p_0p_y & S(p_y^2 + p_x^2) + Np_z^2 + 2m_0\Delta_c \end{pmatrix} \quad (1)$$

where L, M, N, Q, R, S, T are effective mass parameters, Δ_c is the crystal field splitting energy, and m_0 the free electron mass. $p_0 = \sqrt{2m_0\Delta_c}$ has been introduced to make the coefficient Λ dimensionless. In Hamiltonian H_0 the basis functions used are X -like, Y -like (Γ_6), and Z -like (Γ_1) functions. If instead, eigenfunctions of valence band angular momentum ($I=1$): $|1,1\rangle = -(1/\sqrt{2})|X + iY\rangle$, $|1,0\rangle = |Z\rangle$, $|1,-1\rangle = (1/\sqrt{2})|X - iY\rangle$ are used as basis states, the Hamiltonian²¹⁻²⁸ gets transformed to

$$H_0 = \frac{1}{2m_0} \begin{pmatrix} P_1 & S & -T \\ S^* & P_3 & -S \\ -T^* & -S^* & P_1 \end{pmatrix}, \quad (2)$$

where $P_1 = \gamma_1 p^2 - \sqrt{2/3}\gamma_2 P_0^{(2)}$, $P_3 = \gamma'_1 p^2 + \sqrt{2/3}\gamma'_2 P_0^{(2)} + 2m_0\Delta_c$, $T = \eta P_{-2}^{(2)} + \delta P_2^{(2)}$, $T^* = \eta P_2^{(2)} + \delta P_{-2}^{(2)}$, $S = \Lambda p_0 P_{-1}^{(1)} + \sqrt{2}\gamma'_3 P_{-1}^{(2)}$, $S^* = -\Lambda p_0 P_1^{(1)} - \sqrt{2}\gamma_3 P_1^{(2)}$, where $P^{(2)}$ and $P^{(1)}$ are second and first rank spherical tensors formed out of the components p_x, p_y, p_z . The new effective mass parameters $\gamma_1, \gamma_2, \gamma'_1, \gamma'_2$, etc., are related to L, M, N , etc., by the relations $\gamma_1 = \frac{1}{3}(L + M + N)$, $\gamma_2 = \frac{1}{3}(L + M - N)$, $\gamma_3 = \frac{1}{6}R$, $\gamma'_1 = \frac{1}{3}(T + 2S)$, $\gamma'_2 = \frac{1}{6}(T - S)$, $\gamma'_3 = \frac{1}{6}Q$, $\eta = \frac{1}{6}(L - M + R)$, $\delta = \frac{1}{6}(L - M - R)$. To take into account the spin-orbit interaction, the basis is enlarged by taking a direct product of the earlier basis $|1,1\rangle, |1,0\rangle, |1,-1\rangle$ and the spin eigenstates

$$\begin{aligned} |u_1\rangle &= |1,1\rangle \left| \frac{1}{2}, \frac{1}{2} \right\rangle, & |u_2\rangle &= |1,0\rangle \left| \frac{1}{2}, \frac{1}{2} \right\rangle, & |u_3\rangle &= |1,-1\rangle \left| \frac{1}{2}, \frac{1}{2} \right\rangle, \\ |u_4\rangle &= |1,1\rangle \left| \frac{1}{2}, -\frac{1}{2} \right\rangle, & |u_5\rangle &= |1,0\rangle \left| \frac{1}{2}, -\frac{1}{2} \right\rangle, & |u_6\rangle &= |1,-1\rangle \left| \frac{1}{2}, -\frac{1}{2} \right\rangle. \end{aligned} \quad (3)$$

The hole Hamiltonian, which is expressed in the above basis is given by

$$H = \begin{pmatrix} H_0 & O \\ O & H_0 \end{pmatrix} + H_{SO}, \quad (4)$$

where O is a 3×3 null matrix and H_{SO} is the Hamiltonian due to the spin-orbit interaction which is given by

$$H_{SO} = \begin{pmatrix} -\lambda & 0 & 0 & 0 & 0 & 0 \\ 0 & 0 & 0 & -\sqrt{2}\lambda & 0 & 0 \\ 0 & 0 & \lambda & 0 & -\sqrt{2}\lambda & 0 \\ 0 & -\sqrt{2}\lambda & 0 & \lambda & 0 & 0 \\ 0 & 0 & -\sqrt{2}\lambda & 0 & 0 & 0 \\ 0 & 0 & 0 & 0 & 0 & -\lambda \end{pmatrix}, \quad (5)$$

where λ characterizes the strength of the interaction. Because of hexagonal symmetry, only the z component of the total angular momentum (orbital, band, and spin) is a constant of motion. Also, the terms linear in p will couple even and odd angular momentum states. Since the boundary of the dot is spherical, the wave functions for the zero SOC can be expanded in terms of spherical Bessel functions as follows:

$$\psi_m = \sum_{n,l} C_{n,l} j_l(k_n^l r) \begin{pmatrix} a_{n,l} Y_{m-1}^l(\theta, \phi) \\ b_{n,l} Y_m^l(\theta, \phi) \\ d_{n,l} Y_{m+1}^l(\theta, \phi) \end{pmatrix}. \quad (6)$$

In Eq. (6), $j_l(x)$ is the spherical Bessel function, $k_n^l = \alpha_n^l/R$, where α_n^l is the n th zero of $j_l(x)$, R is the dot radius, and $C_{n,l}$ is an overall normalization constant given by $C_{n,l} = (\sqrt{2}/R^{3/2})[1/j_l(\alpha_n^l)]$. For finite SOC, the Hamiltonian is given by Eq. (4) and the wave function is expanded as

$$\psi_{m+1/2} = \sum_{l,n} C_{n,l} j_l(k_n^l r) \begin{pmatrix} a_{n,l} Y_l^{m-1}(\theta, \phi) \\ b_{n,l} Y_l^m(\theta, \phi) \\ d_{n,l} Y_l^{m+1}(\theta, \phi) \\ a'_{n,l} Y_l^m(\theta, \phi) \\ b'_{n,l} Y_l^{m+1}(\theta, \phi) \\ d'_{n,l} Y_l^{m+2}(\theta, \phi) \end{pmatrix}. \quad (7)$$

It should be noted that the m values in the last three terms of the column matrix, given in Eq. (7), are one more than the corresponding values in the first three, because the former are associated with spin states with $S_z = \frac{1}{2}$ while the later are associated with $S_z = -\frac{1}{2}$. The energy eigenvalues and wavefunctions for the hole states are obtained from the solution of the Schrödinger equation

$$H\Psi_{m+1/2} = E\Psi_{m+1/2} \quad (8)$$

with H given by Eq. (4) and $\Psi_{m+1/2}$ given by Eq. (7).

B. Zinc blende structure

While the basic structure in wurtzite is hexagonal close packed (hcp), the basic structure in zinc blende is face centered cubic (fcc). There are no crystal field effects and also the terms linear in momentum are absent in the zinc blende Hamiltonian. The transitions from the Hamiltonian H_0 in the wurtzite case to the corresponding one in the zinc blende is easily obtained by putting $\Delta_{cr} = 0, \Lambda = 0, R = Q = N, S = M, T = L$. Baldereschi and Lipari⁴⁰ have shown that in the spherical symmetry approximation, the Hamiltonian for hole states for zinc blende structure can be put in the form

$$H = \frac{\gamma_1}{2m_0} \left[p^2 - \frac{\mu}{3} P^{(2)} I^{(2)} \right], \quad (9)$$

where $P^{(2)}$ is the second rank tensor formed out of the momentum components mentioned earlier, $I^{(2)}$ is a second rank tensor representing the angular momentum 1 and γ_1 and μ are given by $\gamma_1 = (L + 2M)/3, \mu = [2(L - 2M) + 3N]/5(L + 2M)$. Solution of the boundary value problem for the hole

states with the Hamiltonian, given in Eq. (9), can now proceed as follows. Since $P^{(2)}$ and $I^{(2)}$ are second rank tensors, a wave function of the form

$$\Psi = \sum_n C_{n,l} a_n j_l(k_n^l r) |(l, I) F, M\rangle + \sum_n C_{n,l+2} b_n j_{l+2}(k_n^{l+2} r) |(l+2, I) F, M\rangle \quad (10)$$

is assumed. As before, $k_n^l R = \alpha_n^l$ is the n th zero of $j_l(x)$. In $|(l, I) F, M\rangle$ the orbital angular momentum l is coupled to angular momentum $I (= 1)$ to obtain F, M being the corresponding z component. Substitution of Ψ in the Schrödinger equation with H given by Eq. (9) leads to secular equations involving the coefficients a_n and b_n , the solution of which yield both the eigenvalues and eigenfunctions of the hole states.

To incorporate the spin-orbit interaction, one can proceed as in the wurtzite case by enlarging the basis to Eq. (3) and adding the spin-orbit interaction given in Eq. (5). However, H_0 contained in Eq. (4) is now the 3×3 matrix representation of the Hamiltonian given by Eq. (9) in the basis $|1, 1\rangle, |1, 0\rangle, |1, -1\rangle$.

But a more convenient way to incorporate the spin-orbit interaction for zinc blende structure under spherical symmetry approximation is to introduce the operator

$$H_{S0} = -2\lambda \vec{I} \cdot \vec{S}, \quad (11)$$

where the parameter λ is the same as in Eq. (5) and is related to the splitting Δ of the valence band at Γ due to the spin-orbit interaction by $\lambda = \Delta/3$. The matrix representation of H_{S0} in the basis of Eq. (3) is identical with the matrix given in Eq. (5). The coupling of spin S with the angular momentum F obtained by coupling l and I gives rise to states characterized by $F' = F \pm \frac{1}{2}$.

$$|F', M'\rangle = \begin{bmatrix} F & \frac{1}{2} & F' \\ M' - \frac{1}{2} & \frac{1}{2} & M' \end{bmatrix} \begin{vmatrix} \frac{1}{2} & \frac{1}{2} \\ \frac{1}{2} & \frac{1}{2} \end{vmatrix} |\Psi_{M'-1/2}^F\rangle + \begin{bmatrix} F & \frac{1}{2} & F' \\ M' + \frac{1}{2} & -\frac{1}{2} & M' \end{bmatrix} \begin{vmatrix} \frac{1}{2} & -\frac{1}{2} \\ \frac{1}{2} & -\frac{1}{2} \end{vmatrix} |\Psi_{M'+1/2}^F\rangle, \quad (12)$$

where the square brackets represent the Clebsch-Gordan (CG) coefficients.⁴¹ The matrix elements of H_{S0} in this basis can be easily worked out by changing the order of coupling through the use of the transformation

TABLE I. The values of the parameters for AlN, GaN, and InN (Refs. 28,42). $\mathbf{k} \cdot \mathbf{p}$ parameters are in the units of $\hbar^2/2m_0$, except A_7 where units are in eV Å.

	AlN	GaN	InN
γ_1	1.92	2.67	3.72
μ	0.7271	0.7191	0.7968
Δ_{cr} (eV)	-0.0932	0.0223	0.0373
Δ_{s0} (eV)	0.0111	0.0111	0.0111
$m_x(m_0)$	0.32	0.20	0.12
$m_z(m_0)$	0.28	0.20	0.12
L	4.171	7.113	10.34
M	0.826	0.627	0.69
N	0.535	0.688	0.741
R	3.758	6.486	9.650
S	0.476	0.581	0.651
T	4.711	7.979	10.841
Q	3.331	6.0543	9.2716
λ	0.456	0.8675	1.0605
A_7	0.096	0.179	0.283
E_g (eV)(hcp)	6.23	3.507	1.994
E_g (eV)(fcc)	4.9	3.299	1.94

$$\begin{aligned}
 & |(l,I)F,S;F',M'\rangle \\
 &= \sum_{I'} U(l,I,F',S;F,I') |l,(I,S),I';F',M'\rangle,
 \end{aligned} \tag{13}$$

where $U(l,I,F',S;F,I')$ are the Racah coefficients.⁴¹ Each of the wave functions Ψ_M in Eq. (12) can now be expanded

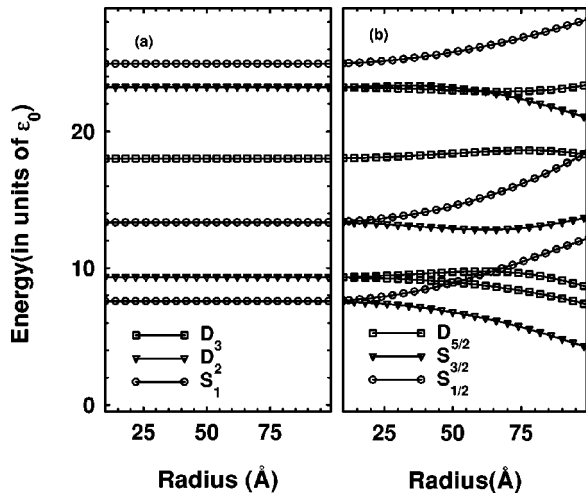


FIG. 1. The energy levels of even parity states in units of $\epsilon_0 = (\gamma_1/2m_0)(\hbar/R)^2$ in a GaN QD with zinc blende structure as a function of dot radius R in (a) zero SOC case (b) finite SOC case. In case (a) (zero SOC), the states are labeled as D_3, D_2, S_1 , etc., where the subscripts represent the total angular momentum $F (=I+I)$ and the capital letters correspond to the lowest l [see Eq. (10)]. In case (b) the subscripts denote the total angular momentum $F' (=F+S)$.

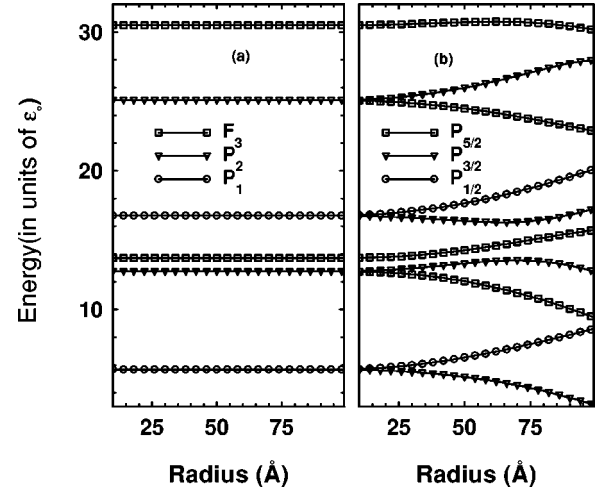


FIG. 2. The energy levels of odd parity states in units of $\epsilon_0 = (\gamma_1/2m_0)(\hbar/R)^2$ in a GaN QD with zinc blende structure as a function of dot radius R in (a) zero SOC case (b) finite SOC.

in terms of spherical Bessel functions and envelope functions $|(l,I)F,M\rangle$ and $|(l+2,I)F,M\rangle$ with $M = M' \pm \frac{1}{2}$ as before [see Eq. (10)] and the corresponding Schrödinger equation can be solved.

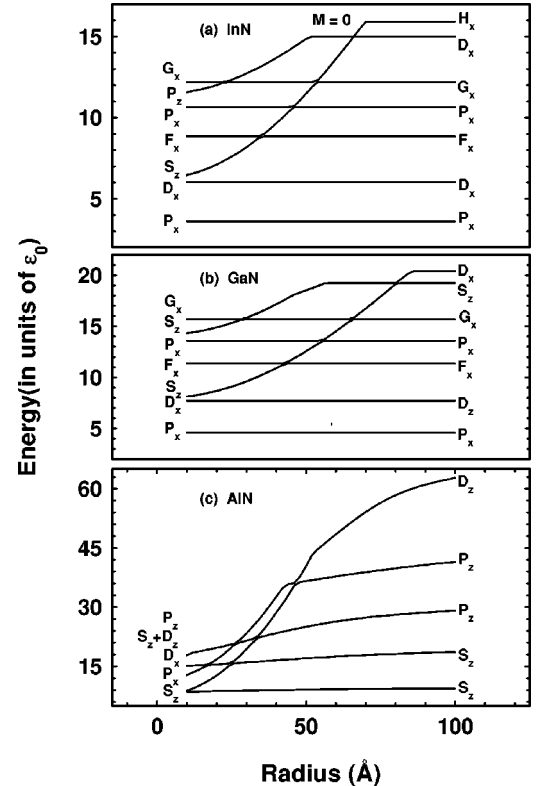


FIG. 3. The energy levels (for $M=0$) in units of ϵ_0 for QD's as a function of dot radius R for (a) InN, (b) GaN, (c) AlN with wurtzite structure in the case of zero SOC. The states are labeled as S_z, P_x , etc., where the capital letters correspond to the dominant l present and the subscripts indicate whether the states are X-, Y-like, or Z-like. The detailed structure of the states are given in Tables II and III.

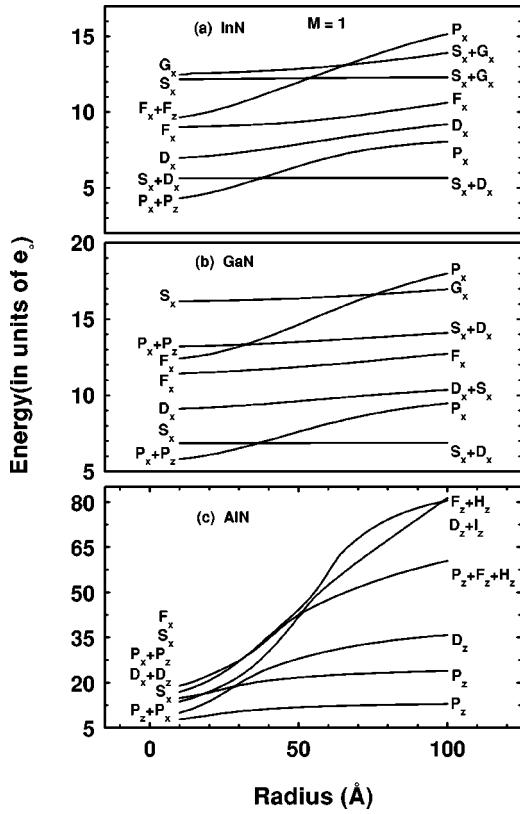


FIG. 4. The energy levels (for $M=1$) in units of ϵ_0 for QD's as a function of dot radius R for (a) InN, (b) GaN, (c) AlN with wurtzite structure in the case of zero SOC.

III. RESULTS AND DISCUSSION

We have calculated and compared the hole state energy eigenvalues and eigenfunctions in the absence, as well as in the presence of SOC for two distinct crystal structures: zinc blende and wurtzite for GaN, InN, and AlN. The difference in the wurtzite and zinc blende Hamiltonians are seen clearly from a comparison of Eqs. (1), (2), and (9). Whereas the zinc blende Hamiltonian in the spherical approximation [Eq. (9)] is characterized by two mass parameters γ_1 and μ , in the wurtzite case more parameters are required. This is because the basic structure changes from fcc in the former to hcp in the later in which a strong crystal field splitting is present. The Z-like states belong to the Γ_1 representation and X, Y-like states belong to the Γ_6 representation. The sign of the crystal field splitting Δ_{cr} is taken positive if Γ_6 (X,Y-like) states lie above Γ_1 (Z-like) states in the valence band as in the case of GaN and InN. The parameter γ_1 is related to the average energy and μ is related to the amount of splitting of the two bands. The values of the parameters γ_1 , μ , Δ_{cr} , and Δ_{SO} (spin-orbit splitting) for GaN, InN, and AlN are given in Table I.^{28,42} Also listed in the table are the effective mass parameters L, M, N, Q, R, S, T and the bulk band gaps of AlN, GaN, and InN.

A. Zero SOC case

We first compare the energy eigenvalues and eigenfunctions for zinc blende and wurtzite structures in the absence of

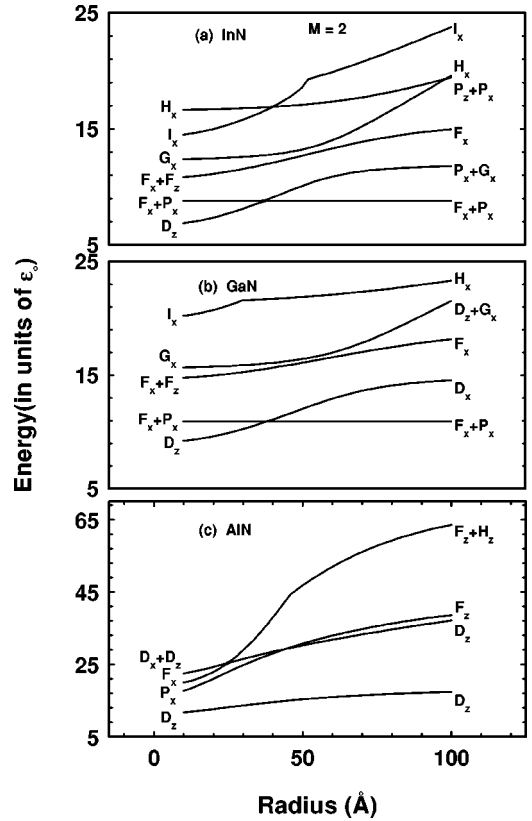


FIG. 5. The energy levels (for $M=2$) in units of ϵ_0 for QD's as a function of dot radius R for (a) InN, (b) GaN, (c) AlN with wurtzite structure in the case of zero SOC.

SOC. As is evident from Table I, the spin orbit effect is much smaller than crystal field effect in AlN, GaN, and InN. Later we shall consider the changes in the trends in eigenvalues and eigenfunctions when the spin-orbit effect is added. The hole energy spectra for GaN as a function of the dot radius for the zinc blende structure are shown in Fig. 1(a) (even parity states), and Fig. 2(a) (odd parity states). Similar trends are observed for InN and AlN. The hole energy eigenvalues for InN, GaN, and AlN for the wurtzite structure are given in Figs. 3, 4, and 5. The zinc blende Hamiltonian (12) is spherically symmetric and the total angular momentum $\vec{F} = \vec{l} + \vec{s}$ is conserved. So the states in Figs. 1(a) and 2(a) are labeled as S_1, D_2, D_3 , etc., where the capital letters correspond to the lowest component of orbital angular momentum present in the state and the subscripts represent the value of \vec{F} . In the case of wurtzite only the z component of angular momentum M is a good quantum number. Figures 3, 4, and 5 correspond to $M=0, 1$, and 2 , respectively. All the energies are in units of $\epsilon_0 = (\gamma_1/2m_0)(\hbar/R)^2$. It is observed from Figs. 1(a) and 2(a) that in the zinc blende zero SOC case the plots of energies (in units of ϵ_0) are horizontal straight lines indicating a strict $1/R^2$ dependence. This is expected because all the elements in the Hamiltonian matrix for zinc blende have a $1/R^2$ dependence. This behavior is modified when the spin orbit interaction is added and the curves show a slope for large R as seen from Figs. 1(b) and 2(b). The spin-orbit contribution

TABLE II. The probabilities of different components for $\mathbf{M}=0$ in the low lying states, starting from the ground state, of wurtzite QD's of AlN, GaN, and InN for radii $R=16 \text{ \AA}$ and $R=76 \text{ \AA}$ in the zero SOC case. For example in state 2 in AlN $(P, +1)=0.49$ indicates that the probability of the component with $l=1$ and $I=1$, $I_z=+1$ is 0.49. The table illustrates how the structure of the states changes with QD radius and material.

AlN		GaN		InN	
$R=16 \text{ \AA}$	$R=76 \text{ \AA}$	$R=16 \text{ \AA}$	$R=76 \text{ \AA}$	$R=16 \text{ \AA}$	$R=76 \text{ \AA}$
$(S, +0)=0.82$	$(S, +0)=0.93$	$(P, +1)=0.49$	$(P, +1)=0.49$	$(P, +1)=0.49$	$(P, +1)=0.49$
		$(P, -1)=0.49$	$(P, -1)=0.49$	$(P, -1)=0.49$	$(P, -1)=0.49$
$(P, +1)=0.49$	$(S, +0)=0.55$	$(D, +1)=0.49$	$(D, +1)=0.49$	$(D, +1)=0.49$	$(D, +1)=0.49$
$(P, -1)=0.49$	$(D, +0)=0.34$	$(D, -1)=0.49$	$(D, -1)=0.49$	$(D, -1)=0.49$	$(D, -1)=0.49$
$(D, +1)=0.49$	$(P, +0)=0.72$	$(S, +0)=0.58$	$(F, +1)=0.49$	$(S, +0)=0.42$	$(F, +1)=0.49$
$(D, -1)=0.49$	$(F, +0)=0.17$	$(S, +0)=0.22$	$(F, -1)=0.49$	$(S, +0)=0.34$	$(F, -1)=0.49$
$(S, +0)=0.68$	$(P, +0)=0.46$	$(F, +1)=0.49$	$(P, +1)=0.49$	$(F, +1)=0.49$	$(P, +1)=0.49$
$(D, +0)=0.20$	$(F, +0)=0.38$	$(F, -1)=0.49$	$(P, -1)=0.49$	$(F, -1)=0.49$	$(P, -1)=0.49$
$(P, +0)=0.51$	$(S, +0)=0.23$	$(P, +1)=0.49$	$(G, +1)=0.45$	$(P, +1)=0.49$	$(G, +1)=0.49$
$(F, +0)=0.14$	$(D, 0)=0.34$	$(P, -1)=0.49$	$(G, -1)=0.45$	$(P, -1)=0.49$	$(G, -1)=0.49$

is independent of R and in units of ϵ_0 , gets multiplied by R^2 causing an increase for large R .

The graphs of the eigenvalues for the wurtzite structure, in the zero SOC case, given in Figs. 3, 4, 5 show the following trends. (i) The lowest curves are completely flat for large R , but as the radius is decreased the curves show a downward slope before becoming flat for very small R again. (ii) As one goes up in energy, the transitions seem to be occurring for higher R . (iii) At larger radii, for InN and GaN (materials with positive crystal field splitting) the lower eigenfunctions are mixtures of $|1,1\rangle$ and $|1,-1\rangle$ states whereas in the case of AlN (with $-ve \Delta_{cr}$) only the $|1,0\rangle$ component is present. The probabilities of the different l components in the wave function associated with each level are given in Tables II, III, IV (zero SOC). (iv) Because of the presence of terms linear in momentum in the Hamiltonian in the wurtzite case, the eigenstates are, in general, mixtures of different parities but the lowest states are seen to be states of definite parity. (v) The lowest states in GaN, InN are P states and not S states whereas the lowest state in AlN is an S state. (vi) The states for small values of the dot radius on the other hand, are

mixtures of all the three states $|1,1\rangle$, $|1,0\rangle$, and $|1,-1\rangle$. (vii) The same is true for the higher excited states for large values of R and (viii) the ground state energy in AlN is much higher than in GaN and InN.

All the features described above can be understood by analyzing the Hamiltonians given in Eqs. (1) and (9). The R dependence of the terms in Eq. (1) have the general form $A/R^2 + \Lambda(B/R) + \Delta_{cr}C$, where $\hbar k = \hbar(\alpha'_n/R)$. Since the energy eigenvalues are in units of $\epsilon_0 = (\gamma_1/2m_0)(\hbar/R)^2$, the observed trends can be clearly understood by representing Hamiltonian given in Eq. (1) in units of ϵ_0 . The Hamiltonian in the basis $|X\rangle$, $|Y\rangle$, $|Z\rangle$, with the matrix elements in the general form highlighting the R dependence is

$$H_0 = \begin{pmatrix} A_1 & A_2 & A_3 + \Lambda BR \\ A_2 & A_1 & A_3 + \Lambda BR \\ A_3 + \Lambda BR & A_3 + \Lambda BR & A'_1 + \Delta_{cr}CR^2 \end{pmatrix}. \quad (14)$$

For GaN and InN, Δ_{cr} is $+ve$ and X -, Y -like states are lower in energy compared to Z -like states ($A_1 < A'_1$). Hence for

TABLE III. The probabilities of different components for $\mathbf{M}=1$ in the low lying states, starting from the ground state, of wurtzite QD's of AlN, GaN, and InN for radii $R=16 \text{ \AA}$ and $R=76 \text{ \AA}$ in the zero SOC case.

AlN		GaN		InN	
$R=16 \text{ \AA}$	$R=76 \text{ \AA}$	$R=16 \text{ \AA}$	$R=76 \text{ \AA}$	$R=16 \text{ \AA}$	$R=76 \text{ \AA}$
$(P, +1)=0.34$	$(P, +0)=0.92$	$(P, +1)=0.54$	$(S, +1)=0.65$	$(P, +1)=0.53$	$(S, +1)=0.54$
$(P, +0)=0.65$		$(P, +0)=0.45$	$(D, -1)=0.32$	$(P, +0)=0.46$	$(D, -1)=0.40$
$(S, +1)=0.83$	$(P, +0)=0.65$	$(S, +1)=0.67$	$(P, +1)=0.77$	$(S, +1)=0.57$	$(P, +1)=0.66$
	$(F, +0)=0.23$	$(D, -1)=0.30$		$(D, -1)=0.38$	$(F, -1)=0.16$
$(D, +1)=0.53$	$(D, +0)=0.82$	$(D, +1)=0.49$	$(D, +1)=0.43$	$(D, +1)=0.52$	$(D, +1)=0.51$
$(D, -1)=0.26$		$(D, -1)=0.19$	$(S, +1)=0.32$	$(D, -1)=0.18$	$(S, +1)=0.27$
$(P, +1)=0.31$	$(F, +0)=0.31$	$(F, -1)=0.52$	$(F, +1)=0.36$	$(F, -1)=0.56$	$(F, +1)=0.40$
$(P, +0)=0.26$	$(H, +0)=0.21$	$(P, +1)=0.16$	$(F, -1)=0.45$	$(P, +1)=0.23$	$(F, -1)=0.36$
$(S, +1)=0.67$	$(D, +0)=0.32$	$(F, +1)=0.38$	$(S, +1)=0.59$	$(F, +1)=0.31$	$(S, +1)=0.49$
$(D, -1)=0.27$	$(I, +0)=0.31$	$(F, +0)=0.18$	$(D, +1)=0.22$	$(F, +0)=0.20$	$(G, -1)=0.29$

TABLE IV. The probabilities of different components for $M=2$ in the low lying states, starting from the ground state, of wurtzite QD's of AlN, GaN, and InN for radii $R=16 \text{ \AA}$ and $R=76 \text{ \AA}$ in the zero SOC case.

AlN		GaN		InN	
$R=16 \text{ \AA}$	$R=76 \text{ \AA}$	$R=16 \text{ \AA}$	$R=76 \text{ \AA}$	$R=16 \text{ \AA}$	$R=76 \text{ \AA}$
$(D, +0)=0.77$	$(D, +0)=0.94$	$(D, +0)=0.64$	$(F, -1)=0.44$	$(D, +0)=0.65$	$(F, -1)=0.46$
$(D, +1)=0.21$		$(D, +1)=0.34$	$(P, +1)=0.51$	$(D, +1)=0.34$	$(P, +1)=0.50$
$(P, +1)=0.70$	$(D, +0)=0.75$	$(P, +1)=0.51$	$(D, +1)=0.50$	$(P, +1)=0.50$	$(D, +1)=0.39$
$(F, +0)=0.15$	$(I, +0)=0.13$	$(F, -1)=0.44$	$(G, -1)=0.2$	$(F, -1)=0.47$	$(G, -1)=0.34$
$(F, +1)=0.34$	$(F, +0)=0.82$	$(F, +1)=0.47$	$(F, +1)=0.53$	$(F, +1)=0.43$	$(F, +1)=0.51$
$(F, -1)=0.33$		$(F, +0)=0.30$	$(F, +0)=0.13$	$(F, +0)=0.36$	$(H, -1)=0.16$
$(D, +0)=0.31$	$(F, +0)=0.46$	$(G, -1)=0.50$	$(D, +0)=0.32$	$(G, -1)=0.53$	$(P, +0)=0.25$
$(D, +1)=0.22$	$(H, +0)=0.28$	$(D, +1)=0.22$	$(G, -1)=0.28$	$(D, +1)=0.22$	$(P, +1)=0.18$
$(G, +1)=0.23$	$(H, +0)=0.28$	$(I, +1)=0.29$	$(H, -1)=0.44$	$(I, +1)=0.23$	$(H, -1)=0.39$
$(G, -1)=0.38$	$(F, +0)=0.21$	$(I, -1)=0.35$	$(H, +1)=0.23$	$(I, -1)=0.28$	$(H, +1)=0.26$

large R , the low lying states will be determined by $H_{11}, H_{12}, H_{21}, H_{22}$ which are constant terms in the matrix given in Eq. (14). This explains (i) the flatness of the curves at large R and (ii) the ground and low lying states are mixtures of $|1,1\rangle$ and $|1,-1\rangle$ only in GaN and InN. In AlN, on the other hand, Δ_{cr} is $-ve$ and Z -like states are lower in energy than X -, Y -like states ($A_1 > A'_1$). The low lying states for large R in AlN should thus have only the $|1,0\rangle$ component as is obtained from the calculation (given in Tables II–IV).

For QD's having the wurtzite structure, the axial component of the total angular momentum M is conserved and M

$=0$ for the lowest eigenfunction. Since $M=l_z+I_z$ and I_z is $+1$ or -1 for the lowest state in GaN, InN (being linear combinations of $|1,1\rangle$ and $|1,-1\rangle$) an $M=0$ state must also have l_z as -1 or $+1$. The lowest l for which this can happen is $l=1$. For AlN on the other hand $I_z=0$ for the lowest state and $M=0$ will be obtained from $l_z=0$ and this can come from an S state. These observations are consistent with the result that the ground state in AlN is an S state while the ground states in GaN and InN are P states. The $|1,1\rangle$ and $|1,-1\rangle$ states being linear combinations of X -, Y -like states

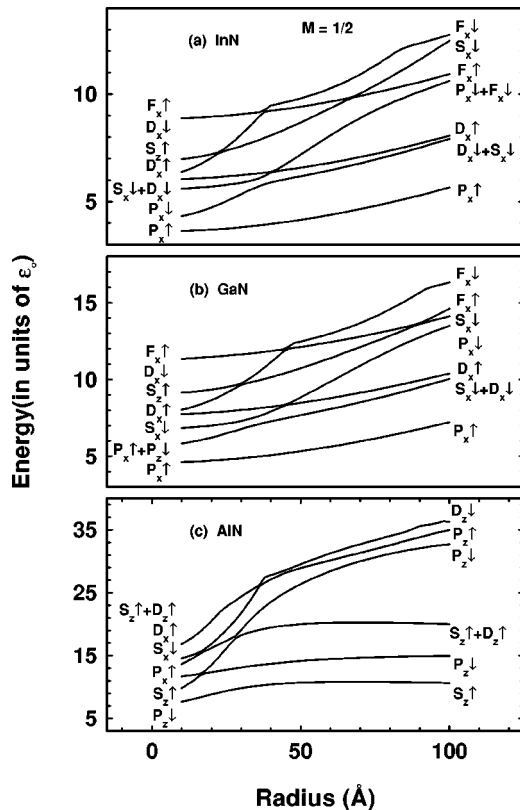


FIG. 6. The energy levels in units of ϵ_0 as a function of the dot radius for (a) InN, (b) GaN, (c) AlN with wurtzite structure in case of finite SOC for $M=\frac{1}{2}$.

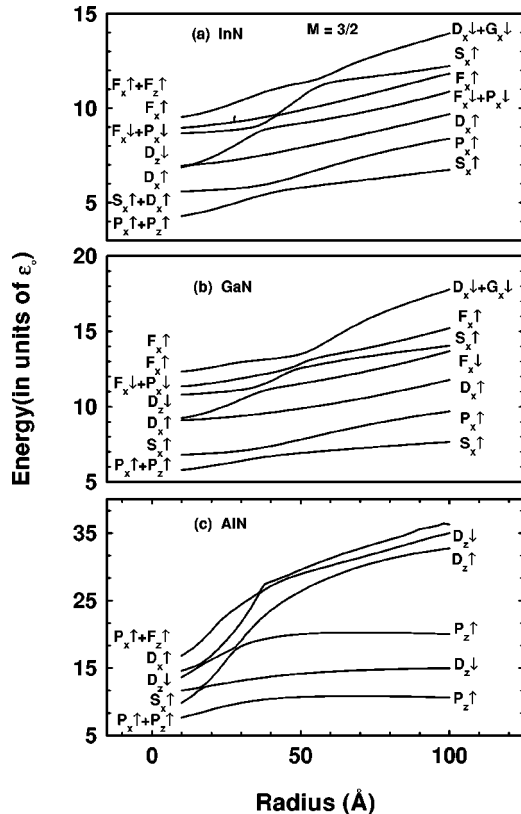


FIG. 7. The energy levels in units of ϵ_0 as a function of the dot radius for (a) InN, (b) GaN, (c) AlN with wurtzite structure in the case of finite SOC for $M=\frac{3}{2}$.

TABLE V. The probabilities of different components for $\mathbf{M}=\frac{1}{2}$ in the low lying states, starting from the ground state, of wurtzite QD's of AlN, GaN, and InN for radii $R=16 \text{ \AA}$ and $R=76 \text{ \AA}$ in the presence of SOC. Now the probabilities also include the spin components indicated by an arrow.

AlN		GaN		InN	
$R=16 \text{ \AA}$	$R=76 \text{ \AA}$	$R=16 \text{ \AA}$	$R=76 \text{ \AA}$	$R=16 \text{ \AA}$	$R=76 \text{ \AA}$
$(P, +1, \downarrow)=0.24$	$(S, +0, \uparrow)=0.86$	$(P, +1, \uparrow)=0.50$	$(P, +1, \uparrow)=0.54$	$(P, +1, \uparrow)=0.50$	$(P, +1, \uparrow)=0.53$
$(P, +0, \downarrow)=0.51$		$(P, -1, \uparrow)=0.49$	$(P, -1, \uparrow)=0.42$	$(P, -1, \uparrow)=0.49$	$(P, -1, \uparrow)=0.44$
$(S, +0, \uparrow)=0.63$	$(P, +0, \downarrow)=0.85$	$(P, +1, \downarrow)=0.52$	$(S, +1, \downarrow)=0.46$	$(P, +1, \downarrow)=0.51$	$(S, +1, \downarrow)=0.43$
$(P, +0, \downarrow)=0.15$		$(P, +0, \downarrow)=0.44$	$(D, -1, \downarrow)=0.3$	$(P, +0, \downarrow)=0.46$	$(D, -1, \downarrow)=0.45$
$(P, +1, \uparrow)=0.51$	$(S, +0, \uparrow)=0.50$	$(S, +1, \downarrow)=0.63$	$(D, +1, \uparrow)=0.55$	$(S, +1, \downarrow)=0.56$	$(D, +1, \uparrow)=0.54$
$(P, -1, \uparrow)=0.49$	$(D, +0, \uparrow)=0.30$	$(D, -1, \downarrow)=0.30$	$(D, -1, \uparrow)=0.40$	$(D, -1, \downarrow)=0.38$	$(D, -1, \uparrow)=0.42$
$(S, +1, \downarrow)=0.79$	$(P, +0, \downarrow)=0.59$	$(D, +1, \uparrow)=0.52$	$(P, +1, \downarrow)=0.52$	$(D, +1, \uparrow)=0.51$	$(P, +1, \downarrow)=0.49$
		$(D, -1, \uparrow)=0.48$	$(F, -1, \downarrow)=0.12$	$(D, -1, \uparrow)=0.48$	$(F, -1, \downarrow)=0.25$
$(D, +1, \uparrow)=0.53$	$(P, +0, \uparrow)=0.63$	$(S, +0, \uparrow)=0.8$	$(S, +1, \downarrow)=0.37$	$(S, +0, \uparrow)=0.8$	$(F, +1, \uparrow)=0.53$
$(D, -1, \uparrow)=0.32$			$(D, +1, \downarrow)=0.20$		$(F, -1, \uparrow)=0.42$

are spatially more spread out than the Z -like states which are confined to a narrow region surrounding the z axis. This confinement may also explain the higher ground state energy in the case of AlN.

In case of the zinc blende Hamiltonian $\Lambda=0$, $\Delta_{\text{cr}}=0$, $A_1=A'_1$, and $A_2=A_3$. Thus all the terms in the Hamiltonian matrix given in Eq. (14) are constant and we get straight curves in units of ϵ_0 , as shown in Figs. 1(a) and 2(a). Also, we observe that the three directions x, y, z are equivalent and hence the ground and low lying states are mixtures of all the three states $|1, 1\rangle$, $|1, 0\rangle$, and $|1, -1\rangle$. Very high excited states have large momentum-dependent contributions. In the case of wurtzite, for very high excited states the effects of Δ_{cr} term becomes negligible compared to momentum dependent contributions and hence the spectrum approaches the zinc blende spectrum as is indicated by the presence of all the three components $|1, 1\rangle$, $|1, 0\rangle$, and $|1, -1\rangle$ in the eigenstates for the flat portions of the graphs obtained for wurtzite structures. For very small R , the effects of the Δ_{cr} term also become negligible. The spectrum will again approach that of zinc blende. In the intermediate R region the $1/R^2$ behavior

represented by straight line in ϵ_0 units, is not observed because effects due to the momentum dependent terms and crystal field term are comparable. Clearly for higher excited states this transition will occur at higher R .

B. Results with SOC

The III-V nitrides have low spin orbit interaction. In the wurtzite structures of these nitrides the spin orbit splitting is smaller than the crystal field splitting (see Table I). The spin orbit interaction part will add terms in the Hamiltonian given in Eq. (1) which are independent of R . Expressed in units of ϵ_0 , these terms will increase as R^2 . The hole energy spectra for GaN as a function of the dot radius for the zinc blende structure in the presence of SOC are shown in Fig. 1(b) (even parity states) and Fig. 2(b) (odd parity states). Contrary to the results in the zero SOC case the energies in units of ϵ_0 are no longer constants as a function of R indicating deviation from $1/R^2$ behavior.

The hole energy spectra for InN, GaN, and AlN for $M=\frac{1}{2}$ and $M=\frac{3}{2}$ as a function of the radius of the QD's are

TABLE VI. The probabilities of different components for $\mathbf{M}=\frac{3}{2}$ in the low lying states, starting from the ground state, of wurtzite QD's of AlN, GaN, and InN for radii $R=16 \text{ \AA}$ and $R=76 \text{ \AA}$ in the presence of SOC.

AlN		GaN		InN	
$R=16 \text{ \AA}$	$R=76 \text{ \AA}$	$R=16 \text{ \AA}$	$R=76 \text{ \AA}$	$R=16 \text{ \AA}$	$R=76 \text{ \AA}$
$(P, +1, \uparrow)=0.32$	$(P, +0, \uparrow)=0.86$	$(P, +1, \uparrow)=0.52$	$(S, +1, \uparrow)=0.78$	$(P, +1, \uparrow)=0.52$	$(S, +1, \uparrow)=0.70$
$(P, +0, \uparrow)=0.64$		$(P, +0, \uparrow)=0.43$	$(D, -1, \uparrow)=0.12$	$(P, +0, \uparrow)=0.46$	$(D, -1, \uparrow)=0.22$
$(S, +1, \uparrow)=0.78$	$(D, +0, \downarrow)=0.88$	$(S, +1, \uparrow)=0.66$	$(P, +1, \uparrow)=0.71$	$(S, +1, \uparrow)=0.59$	$(P, +1, \uparrow)=0.70$
		$(D, -1, \uparrow)=0.28$		$(D, -1, \uparrow)=0.36$	
$(D, +0, \downarrow)=0.76$	$(P, +0, \uparrow)=0.60$	$(D, +1, \uparrow)=0.49$	$(D, +1, \uparrow)=0.52$	$(D, +1, \uparrow)=0.53$	$(D, +1, \uparrow)=0.57$
$(D, +1, \downarrow)=0.19$	$(F, +0, \uparrow)=0.21$	$(D, -1, \uparrow)=0.20$	$(D, -1, \uparrow)=0.29$	$(D, +0, \uparrow)=0.17$	$(D, -1, \uparrow)=0.20$
$(D, +1, \uparrow)=0.37$	$(D, +0, \uparrow)=0.69$	$(D, +1, \downarrow)=0.33$	$(F, +1, \downarrow)=0.44$	$(D, +1, \downarrow)=0.33$	$(F, -1, \downarrow)=0.48$
$(D, -1, \uparrow)=0.20$		$(D, +0, \downarrow)=0.64$	$(F, -1, \downarrow)=0.44$	$(D, +0, \downarrow)=0.65$	$(P, 1, \downarrow)=0.43$
$(P, +1, \uparrow)=0.238$	$(D, +0, \downarrow)=0.65$	$(F, -1, \downarrow)=0.44$	$(S, +1, \uparrow)=0.44$	$(F, -1, \downarrow)=0.46$	$(F, +1, \uparrow)=0.39$
$(D, +1, \uparrow)=0.16$		$(P, +1, \downarrow)=0.51$	$(D, +1, \uparrow)=0.15$	$(P, +1, \downarrow)=0.48$	$(F, -1, \uparrow)=0.39$

shown in Figs. 6(a), 6(b), and 6(c) and Figs. 7(a), 7(b), and 7(c), respectively. The probabilities of the different l components in the wave function associated with each level are given in Tables II, III, IV (zero SOC) and Tables V, VI (with SOC). For values of R in the range 25–50 Å, energy eigenvalues trend is a bit complicated and level crossings seem to occur. For GaN, for example, the second excited state in the $M = \frac{1}{2}$ case, changes from a P state for small R 15 Å to a mixture of S and D states for R 80 Å. For AlN the crossing of levels take place at a much lower value of R than in GaN and InN.

As in the zero SOC case, in GaN and InN, the lower states in the spectra for large R are mixtures of $|1,1\rangle$ and $|1,-1\rangle$ states but for lower R $|1,0\rangle$ state also appears (given in Tables V and VI). But unlike the zero SOC case, the curves are not horizontal lines for large R , as seen in Figs. 6, 7. For GaN and InN the curves have an upward slope but for AlN the curve is somewhat flatter. This can be understood from the fact that in GaN and InN the crystal field and the spin-orbit effects add up. Since these terms in the Hamiltonian are independent of R , in units of ϵ_0 their effect increase as R^2 giving rise to an upward slope for large R . In AlN, Δ_{cr} is negative and the crystal field and spin orbit effect partially cancel each other giving rise to a somewhat flatter spectrum for large R . In all the three material the lowest state correspond to $M = \frac{1}{2}$. The band gap as a function of radius of the QD is plotted for both the zinc blende and wurtzite structures in Fig. 8.

IV. CONCLUSIONS

The electronic structure of QD's of the III-V nitrides InN, GaN, and AlN have been studied for both the zinc blende and wurtzite structures. The following has been found.

(1) The energies for the zinc blende structure as a function of dot radius R has a strict $1/R^2$ dependence for zero SOC. In the presence of SOC the energies fall off more slowly and do not follow strict $1/R^2$ dependence at large R .

(2) For the wurtzite structure the energies vary as $1/R^2$ for very large and very small R in the zero SOC case. In the intermediate region the effects due to the crystal field terms

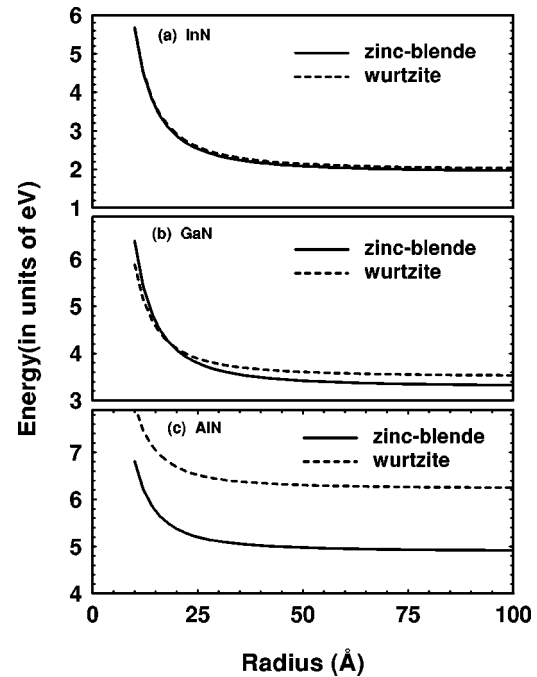


FIG. 8. Band gap in units of eV as a function of the dot radius R for (a) InN, (b) GaN, (c) AlN with zinc blende as well as wurtzite structure with finite SOC.

and the linear terms in the Hamiltonian become important and the R dependence is more complex.

(3) Similar to the zinc blende case in wurtzite with SOC, the energies fall off more slowly than $1/R^2$ for large values of R . The deviation from the $1/R^2$ behavior for large R is much less in AlN than in GaN and InN. This is because in the case of AlN, Δ_{cr} is negative and partially cancels the spin-orbit effect.

(4) The lowest states in GaN and InN materials are P states and not S states whereas for AlN the lowest state is an S state.

(5) The eigenstates and the eigenvalues with wurtzite structure approach those for the zinc blende structure for very high excited states of large quantum dots and also for quantum dots with very small radius, though the effective mass theory breaks down at very small radius.

¹K.P. O'Donnell, R.W. Martin, and P.G. Middleton, Phys. Rev. Lett. **82**, 237 (1999); M. Grundmann, Physica E (Amsterdam) **5**, 167 (2000).

²W. Wegscheider, G. Schedelbeck, M. Bichler, and G. Abstreiter, Physica E (Amsterdam) **3**, 103 (1998).

³D. Goldhaber-Gordon, Hadas Shtrikman, D. Mahalu, David Abusch-Magder, U. Meirav, and M.A. Kastner, Nature (London) **391**, 156 (1998).

⁴C.P. Collier, S. Honrichs, J.J. Shiang, R.J. Saykally, and J.R. Heath, Science **277**, 1978 (1997).

⁵Huajie Chen, R.M. Feenstra, J.E. Northrup, T. Zywiez, and J. Neugebauer, Phys. Rev. Lett. **85**, 1902 (2000).

⁶B. Daudin, F. Widmann, G. Feuillet, Y. Samson, M. Arlery, and

J.L. Rouviere, Phys. Rev. B **56**, R7069 (1997).

⁷R. Rossetti, R. Hull, and L.E. Brus, J. Chem. Phys. **82**, 552 (1985).

⁸N. Chestnoy, R. Hull, and L.E. Brus, J. Chem. Phys. **85**, 2237 (1986).

⁹Satoru Tanaka, Hideki Hirayama, Yoshinobu Aoyagi, Yukio Narukawa, Yoichi Kawakami, and Shigeo Fujita, Appl. Phys. Lett. **71**, 1299 (1997).

¹⁰Satoru Tanaka, Hideki Hirayama, and Yoshinobu Aoyagi, Appl. Phys. Lett. **69**, 4096 (1996).

¹¹F. Widmann, J. Simon, D. Daudin, G. Feuillet, J.L. Rouviere, N.T. Pelekanos, and G. Fishman, Phys. Rev. B **58**, 15 989 (1998).

¹²A.D. Andreev and E.O. O'Reilly, Phys. Rev. B **62**, 15 851 (2000).

- ¹³V. Lemos, E. Silveira, J.R. Leite, A. Tabata, R. Trentin, L.M.R. Scolfaro, T. Frey, D.J. As, D. Schikora, and K. Lischka, *Phys. Rev. Lett.* **84**, 3666 (2000).
- ¹⁴I. Ho and G.B. Stringfellow, *Appl. Phys. Lett.* **69**, 2701 (1996).
- ¹⁵S. De Rinaldis, I. D'Amico, E. Biolatti, R. Rinaldi, R. Cingolani, and F. Rossi, *Phys. Rev. B* **65**, 081309(R) (2002).
- ¹⁶W.D. Oliver, F. Yamaguchi, and Y. Yamamoto, *Phys. Rev. Lett.* **88**, 037901 (2002).
- ¹⁷C.B. Murray, D.J. Norris, and M.G. Bawendi, *J. Am. Chem. Soc.* **115**, 8706 (1993).
- ¹⁸A.I. Ekimov, F. Hache, M.C. Schanne-Klein, D. Ricard, C. Flytzanis, I.A. Kudryavtsev, T.V. Yazeva, A.V. Rodina, and Al.L. Efros, *J. Opt. Soc. Am. B* **10**, 100 (1993).
- ¹⁹Al.L. Efros, M. Rosen, M. Kuno, M. Nirmal, D.J. Norris, and M. Bawendi, *Phys. Rev. B* **54**, 4843 (1996).
- ²⁰U. Banin, C.J. Lee, A.A. Guzelian, A.V. Kadavanich, A.P. Alivisatos, W. Jaskolski, G.W. Bryant, Al.L. Efros, and M. Rosen, *J. Chem. Phys.* **109**, 2306 (1998).
- ²¹K. Chang and J.B. Xia, *J. Appl. Phys.* **84**, 1454 (1998).
- ²²K. Chang and J.B. Xia, *Phys. Rev. B* **57**, 9780 (1998).
- ²³J.B. Xia and J.B. Li, *Phys. Rev. B* **60**, 11 540 (1999).
- ²⁴J. Li and J.B. Xia, *Phys. Rev. B* **61**, 15 880 (2000).
- ²⁵J.B. Xia, *J. Lumin.* **70**, 120 (1996).
- ²⁶J.B. Xia, K.W. Cheah, X.L. Wang, D.Z. Sun, and M.Y. Kang, *Phys. Rev. B* **59**, 10 119 (1999).
- ²⁷M. Suzuki, T. Uenoyama, and A. Yanase, *Phys. Rev. B* **52**, 8132 (1995).
- ²⁸D.J. Dugdale, S. Brand, and R.A. Abram, *Phys. Rev. B* **61**, 129393 (2000).
- ²⁹Serdar Ogut, J.R. Chelikowsky, and S.G. Louie, *Phys. Rev. Lett.* **79**, 1770 (1997).
- ³⁰A. Franceschetti, H. Fu, L.W. Wang, and A. Zunger, *Phys. Rev. B* **60**, 1819 (1999).
- ³¹A.J. Williamson and A. Zunger, *Phys. Rev. B* **61**, 1978 (2000).
- ³²C. Delerue, G. Allan, and M. Lannoo, *Phys. Rev. B* **48**, 11 024 (1993).
- ³³E. Martin, C. Delerue, G. Allan, and M. Lannoo, *Phys. Rev. B* **50**, 18 258 (1994).
- ³⁴K. Leung and K.B. Whaley, *Phys. Rev. B* **56**, 7455 (1997).
- ³⁵K. Leung, S. Pokrant, and K.B. Whaley, *Phys. Rev. B* **57**, 12 291 (1998).
- ³⁶G. Allan, Y.M. Niquet, and C. Delerue, *Appl. Phys. Lett.* **77**, 639 (2000).
- ³⁷U.E.H. Laheld and G.T. Einevoll, *Phys. Rev. B* **55**, 5184 (1997).
- ³⁸H.H. von Grunberg, *Phys. Rev. B* **55**, 2293 (1997).
- ³⁹L.W. Wang and A. Zunger, *Phys. Rev. B* **53**, 9579 (1996).
- ⁴⁰A. Baldereschi and N.O. Lipari, *Phys. Rev. B* **8**, 2697 (1973).
- ⁴¹A. R. Edmonds, *Angular Momentum in Quantum Mechanics* (Princeton University Press, Princeton, 1960).
- ⁴²I. Vurgaftman, J.R. Meyer, and L.R. Ram-Mohan, *J. Appl. Phys.* **89**, 5815 (1998).